PAPER • OPEN ACCESS

A novel method for treating MAR in EMC3-Eirene, and first applications to W7-X

OPEN ACCESS
IOP Publishing | International Atomic Energy Agency
Nuclear Fusion
Nucl. Fusion **65** (2025) 066008 (12pp)
https://doi.org/10.1088/1741-4326/add27a

A novel method for treating MAR in EMC3-Eirene, and first applications to W7-X

Y. Feng[1,*], D. Reiter[2], H. Frerichs[3] and the W7-X Team[a]

[1] Max-Planck-Institut für Plasmaphysik, 17491 Greifswald, Germany
[2] Institute for Laser and Plasma Physics, Heinrich-Heine-University, D-40225 Duesseldorf, Germany
[3] Department of Nuclear Engineering & Engineering Physics, University of Wisconsin, Madison, WI, United States of America

E-mail: feng@ipp.mpg.de

Received 24 February 2025, revised 11 April 2025
Accepted for publication 30 April 2025
Published 9 May 2025

Abstract

This paper presents a novel 'prediction-correction method' for treating molecule-assisted recombination (MAR) in the three-dimensional (3D) boundary plasma transport code—EMC3-Eirene. In this approach, certain MAR products are first isolated and removed from the particle trajectories in Eirene and recorded as predictions, which are then implicitly corrected/reprocessed in EMC3 and subsequently fed back into Eirene as an 'external' source to compensate for the removed particles. Compared to the conventional scheme used in boundary plasma modelling, this new method exhibits enhanced numerical stability. It should be broadly applicable to other 2D fluid-kinetic edge plasma transport calculations. Using a typical detached plasma from W7-X as an example, we apply the latest version of the EMC3-Eirene code to perform, for the first time, a self-consistent analysis of the role of volume recombination processes, including MAR and electron–ion recombination (EIR), in a 3D divertor, namely the island divertor. Intrinsic carbon is assumed to be the only impurity species, and the radiation fraction f_{rad} is used as a control parameter. The simulation demonstrates that both EIR and MAR increase with f_{rad}, with the total volume recombination rate reaching approximately 30% of the total neutral source at $f_{\mathrm{rad}} = 0.9$. The MAR contribution is typically around a factor of three of that of the EIR when the radiation is located in the edge magnetic islands outside the last closed flux surface. There are no noteworthy effects of volume recombination on detachment performance regarding the power load on the target, the neutral pressure in the divertor chamber, or the distribution of impurity radiation. Nevertheless, volume recombination significantly changes the relative population of atoms and molecules in front of the targets, which may be generally important for boundary plasma spectroscopy in fusion devices.

[a] See Grulke *et al* 2024 (https://doi.org/10.1088/1741-4326/ad2f4d) for the W7-X Team.
[*] Author to whom any correspondence should be addressed.

Keywords: EMC3-Eirene, prediction-correction method, volume recombination, detachment, MAR

(Some figures may appear in colour only in the online journal)

1. Introduction

The divertor plasma is usually described by combining fluid models for the background plasma with a kinetic model for the recycling neutral gas. One of the most widely used computational tools of this type is the EMC3-Eirene code, which is a coupled code package comprising EMC3 [1] for charged particles and Eirene [2] for neutral particles. The former provides the background plasma on a macroscopic (fluid) level on which the latter calculates the neutral transport and the associated plasma-neutral interactions on a microscopic (kinetic) level. The plasma state variables **P** and neutral gas state variables **N** are iterated until convergence is achieved (operator splitting and fix point iteration). Considering particle balance and in the absence of volume recombination, the background plasma provides a pure sink for the neutral particles due to the processes of ionization and dissociation. These processes are naturally treated as 'collision events' in Eirene, as the corresponding reaction rates are proportional to the density of the neutral particles tracked. In contrast, electron–ion recombination (EIR), which is mainly due to three-body recombination reactions, involving only charged particles, results in a source for the neutral particles. Consequently, this process is treated in the Eirene code as the inhomogeneous term (external source term) in the linear transport equation, as recently included in the EMC3-Eirene code for studying detachment in ITER [3].

As will be discussed in greater detail in section 2, molecule-assisted recombination (MAR) processes [4] consist of a sequence of atomic reactions involving the participation of electrons, ions and molecules. In the conventional linear Monte Carlo procedures the MAR processes result in a net intrinsic volumetric atom source that is proportional not only to plasma density but also to the molecule density. In the present version of the Eirene code, the MAR exit channel is treated as a cascading process, as are all other molecule fragmentation processes. This treatment of the MAR process can, at least under certain conditions, lead to an exponential growth of the neutral particle population (extremely long or even infinite trajectories), with unfavourable consequences for the coupled EMC3-Eirene system. This situation is reminiscent e.g. to intrinsic neutron generation from fission processes and poses a criticality or near-criticality issue [5]. Indeed, a runaway neutral particle generation has occasionally been encountered in some cases when a MAR reaction chain was activated in Eirene during an EMC3-Eirene simulation of W7-X detachment scenarios. As will be demonstrated in this paper, the total MAR contribution to the recycling process is, in fact, rather limited in W7-X. This numerical issue has motivated the development of an alternative approach where one of the MAR products is split off from the neutral gas transport operator as an initial guess (prediction), which is then implicitly corrected in EMC3 and fed back to Eirene as an 'external' source in the subsequent iteration step, hence the name 'prediction-correction' method. Our objective here is to enhance numerical stability rather than to achieve higher integration accuracy, as is the case in the conventional 'predictor-corrector' method employed in ordinary differential equations (see, for example, [6]) . This new 'prediction-correction' method will be presented in a rather schematic way in section 3, following concepts and notation similar to those conventionally used in (fission) neutron criticality studies (so called 'power iterations' for eigenvalues in linear operators), see [5], sections 2–4. There the fission neutrons are split off from the neutron transport operator, re-normalized and iterated. But in our case also the other external neutral gas sources remain active in the computation. Our aim is merely to reduce the spectral range of the collision operator for neutrals, for improved stability of the coupling scheme, rather than true criticality (k-eigenvalue) studies as it is the case in neutronics.

MAR processes are already active at plasma temperatures clearly above those required for EIR—a divertor plasma condition that is more readily attainable than that necessary for an intensive EIR. As a potential for the creation of a so-called gaseous divertor [4], MAR has attracted considerable attention in both tokamaks [7, 8] and linear devices [9, 10], and has been the subject of extensive research. In contrast, there has been a paucity of related studies in stellarators, especially in terms of modelling. The extended version of the EMC3-Eirene code now makes it possible, for the first time, to evaluate the role of volume recombination processes in helical devices. The fourth section will present a detailed analysis of the relevance and significance of EIR and MAR for the W7-X island divertor.

2. Molecule assisted recombination (MAR)

The MAR processes addressed in this work can be classified into two distinct reaction chains. In a hydrogen plasma, the first MAR chain begins with a process of charge exchange (CX, aka: 'charge transfer' or 'ion conversion') between protons and vibrationally excited hydrogen molecules:

$$\mathrm{H}_2\,(\nu) + \underline{\mathrm{H}}^+ \rightarrow \mathrm{H}_2^+ + \underline{\mathrm{H}}.$$

This process becomes resonant and even exothermal for vibrational levels ν at or above four. The formation of ion H_2^+ is then followed by rapid dissociative recombination (DR):

$$\mathrm{H}_2^+ + \mathrm{e} \rightarrow \mathrm{H} + \mathrm{H}.$$

This second step is, at least, a two-step process in itself, because one of the product H atoms is initially formed in an electronically excited state H^*, which then, by further

collisional or radiative transitions, can result in the final neutral H (ground state) atom, completing the MAR sequence. Through the entire chain of two-step (better: multi-step) processes, finally an electron and an ion $\underline{\mathrm{H}}^+$ 'recombine' to form an atom $\underline{\mathrm{H}}$ and the molecule is dissociated into two H atoms. For convenience, henceforth in this paper the recombination process through the H_2^+ ion channel will be referred to as 'CX-MAR' - a term derived from [10]. In addition to the dissociative recombination, there are other reactions that also participate in the breakdown of H_2^+ ions. The most important are the processes of dissociative excitation $\mathrm{H}_2^+ + \mathrm{e} \rightarrow \mathrm{e} + \mathrm{H}^+ + \mathrm{H}$ and dissociative ionization $\mathrm{H}_2^+ + \mathrm{e} \rightarrow 2\mathrm{e} + 2\mathrm{H}^+$, which compete with the MAR sequence.

The second MAR chain under consideration is a combination of the processes of dissociative attachment (DA) and mutual neutralization (MN):

$$\mathrm{H}_2(\nu) + \mathrm{e} \rightarrow \mathrm{H} + \mathrm{H}^-$$
$$\mathrm{H}^- + \underline{\mathrm{H}}^+ \rightarrow \mathrm{H} + \underline{\mathrm{H}}.$$

Here again, in the second step initially one H^* is formed, which can then rapidly decay to H or, in a competing process channel, ionize to H^+. As in [10], this MAR sequence of processes through the H^- channel is designated as 'DA-MAR'. In addition to MN, there are again other reactions that eliminate the intermediate negative hydrogen ion. The two most relevant ones considered in this paper are $\mathrm{H}^- + \mathrm{H}^+ \rightarrow \mathrm{H} + \mathrm{H}^* \rightarrow \mathrm{H} + \mathrm{H}^+ + \mathrm{e}$ and $\mathrm{H}^- + \mathrm{e} \rightarrow \mathrm{H} + 2\mathrm{e}$, respectively.

In the Eirene code, the intermediate H_2^+ and H^- kinetic test particle ions usually do not undergo any transport, but are assumed to remain static until they are eliminated by further collisional processes. This reduced treatment is often plausible given the short lifetime of these ions in typical fusion boundary conditions. Under that assumption of quasi-static H_2^+ and H^-, the two MAR reaction chains can both be combined into a compact single step form of

$$\mathrm{H}_2(\nu) + \underline{\mathrm{H}}^+ + \mathrm{e} \rightarrow \underline{\mathrm{H}} + 2\mathrm{H}(=3\mathrm{H}). \qquad (1)$$

Here, to a good approximation, we assume that the $\underline{\mathrm{H}}$ atom carries momentum and energy of the incident $\underline{\mathrm{H}}^+$ ion from the first (CX) step in CX-MAR, and, for the time being and for simplicity, we make the similar assumption for the second (MN) step in DA-MAR, while the two other H atoms emerge from the other involved process channels, with a different kinetic energy release there. In our context this means that in this reduced (condensed) picture, in both cases with the involvement of H_2, an electron and an ion $\underline{\mathrm{H}}^+$ undergo 'recombination' to $\underline{\mathrm{H}}$, while, simultaneously, H_2 is effectively 'dissociated' into two atoms 2H, although the detailed kinetics of the more correct fuller sequence of events was different. The corresponding volumetric recombination rates can be expressed as $n_{\mathrm{H}_2} n \langle\sigma v\rangle^{\mathrm{cx}}_{\mathrm{mar}}$ and $n_{\mathrm{H}_2} n \langle\sigma v\rangle^{\mathrm{da}}_{\mathrm{mar}}$, respectively, where n_{H_2} is the molecule density and $n \equiv n_\mathrm{e} = n_\mathrm{i}$. The recombination rate coefficients $\langle\sigma v\rangle^{\mathrm{cx}}_{\mathrm{mar}}$ and $\langle\sigma v\rangle^{\mathrm{da}}_{\mathrm{mar}}$ are displayed in figure 1, compared with those of the processes of EIR and H-ionization from electron collisions. They are all given in the AMJUEL format [11] and are taken from published databases or CR-codes (loc.cit).

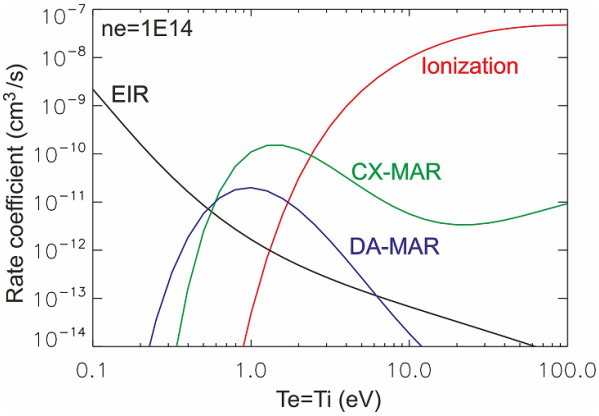

Figure 1. Rate coefficients of CX-MAR, DA-MAR, EIR and ionization of hydrogen atom at $n = 10^{14}$ cm^{-3}, taken from AMJUEL database [11] (loc.cit). Note that they all depend on the plasma density.

While the relative importance of CX-MAR and DA-MAR can be directly compared, vs. n_e and $T_\mathrm{e}(=T_\mathrm{i})$, their importance relative to EIR and the ionization process cannot be immediately assessed without precise knowledge of the ratios of atom and molecule density to plasma density in realistic cases. Therefore, the rate coefficients of EIR and ionization of hydrogen atoms are provided for reference only. Nevertheless, compared to the EIR, which increases rapidly with decreasing plasma temperature below about 1 eV, the MAR processes have maxima in the temperature range of 1 to 2 eV. This characteristic of the MAR processes has implied their potential importance, relative to the EIR, for W7-X, as it has been shown numerically that a downstream plasma with a temperature below 1 eV is difficult to establish in W7-X under the currently available experimental conditions [12].

3. Numerical aspects

3.1. The prediction-correction method

When the recycling neutral particles (atoms and molecules) are considered as a whole, the MAR processes discussed in the foregoing section act as intrinsic particle multiplication processes within the neutral gas component, although they provide a pure local sink for hydrogen molecules. Two of the resulting atoms can recombine at surfaces to form a next generation H_2, and in a given prescribed plasma field $\mathbf{P}$ ($n_\mathrm{e} = n_\mathrm{i}$, as well as temperatures and plasma flows) this can produce the next MAR cycle, resulting in one further new additional neutral atom in the system, and so on, self-amplifying the neutral particle population and fluxes. Hence the population of the induced atoms can exhibit exponential growth depending on the specific conditions of divertor plasma, geometry and materials, when Eirene is operated in a time-independent mode (as it is usually the case). This exponential increase occurs when the probability of ionization and other losses for

these atoms is lower than the probability of conversion into molecules on plasma-facing components (PFCs). These wall recycled molecules then induce repeated MAR (cascading) processes during the lifespan of a neutral particle history from birth to death. This phenomenon may occur only locally, but still resulting in a runaway Monte Carlo particle tracing and reduced overall stability.

Physically, an uncontrolled production of neutral particles through the MAR processes is a consequence of the violation of particle conservation. Eirene is operated in a time-independent mode in a given fixed background plasma. In each Eirene run, the production of atoms from the MAR is taken into account, but the corresponding loss of protons is not. One way to overcome this problem is to move the treatment of the proton-atom conversion process in the MAR chains from Eirene to EMC3, where the loss of protons is implicitly calculated and the corresponding atom yield then remains limited. This idea is implemented numerically by developing a new prediction-correction method.

To outline the basic idea behind the new prediction-correction method we start with a very symbolic form of equations, omitting phase space coordinates $\boldsymbol{x},\boldsymbol{v}$ and also indices of the composition component. For the neutral gas transport equations of Eirene the dependent quantity is $\mathbf{N} := \mathbf{f} = (f_{\mathrm{at}}, f_{\mathrm{mol}}, f_{\mathrm{ti}})$ with the multi-component kinetic phase space distribution $\mathbf{f} = (f_{\mathrm{at}}, f_{\mathrm{mol}}, f_{\mathrm{ti}})$, for atoms (at) molecules (mol) and the intermediate molecular ions or negative ions (ti), in a given bath of ions (i, H^+) and electrons e, with densities n_{i} and n_{e}, respectively. The plasma parameters (solved for by EMC3) are the 3D plasma flow fields $\mathbf{P} = (n, T_{\mathrm{e}}, T_{\mathrm{i}}, u_{\parallel})$, again omitting space coordinates $\boldsymbol{x}$, for notational clarity.

The generic stationary neutral particle transport equation is well known from applications to neutronics, or radiation transfer and many other particle transport problems, and it reads:

$$\mathbf{N} = \mathcal{K}\mathbf{N} + \Gamma. \tag{2}$$

Here $\mathcal{K}$ is a (linear) transport operator, comprising ballistic and collisional transport, surface interactions and particle losses (e.g. ionization, dissociation, etc). Γ is an external source for neutral particles (here, e.g.: EIR, recycling of plasma ions at walls as neutrals, or neutrals from a gas puff). At each iterative step 'i' of the coupled EMC3 – Eirene system all parameters in Eirene appearing in Γ^i and $\mathcal{K}^i$ are fully determined by the plasma state $\mathbf{P}^i$ obtained from EMC3. One single neutral gas step with the Eirene code evaluates

$$\mathbf{N}^i = \Gamma\left(\mathbf{P}^i\right)\left(\mathbb{1} - \mathcal{K}^i\right)^{-1} \tag{3}$$

using conventional Monte Carlo particle transport procedures. In the absence of MAR, the transport operator $\mathcal{K}$ has a spectral radius $r(\mathcal{K})$ less than one, accounting for the loss of neutral particles through ionization, dissociation, pumping, etc to balance the external source Γ. However, in the presence of MAR, the spectral radius $r(\mathcal{K})$ can exceed one and a steady-state solution—equation (3)—may no longer exist (infinite trajectories and exponential growth of $\mathbf{N}^i$). To cope with this potential criticality in the Monte Carlo neutral particle solver, we split off from the operator $\mathcal{K}$ one branch of the cascading trajectory emerging from MAR processes, $\mathcal{K}_{\mathrm{MAR}_{\underline{\mathrm{H}}}}$, while adding an additional 'external' source term $\Gamma_{\mathrm{MAR}_{\mathrm{H}}}$ to compensate, so that

$$\mathcal{K}^i\mathbf{N}^i = \left(\mathcal{K}^i - \mathcal{K}^i_{\mathrm{MAR}_{\underline{\mathrm{H}}}}\right)\mathbf{N}^i + \Gamma^{i-1}_{\mathrm{MAR}_{\mathrm{H}}} = \tilde{\mathcal{K}}^i\mathbf{N}^i + \Gamma^{i-1}_{\mathrm{MAR}_{\mathrm{H}}} \tag{4}$$

holds. $\mathcal{K}^i_{\mathrm{MAR}_{\underline{\mathrm{H}}}}$ describes the contribution of the neutral particle distributions $\mathbf{N}^i$ from trajectories starting from the $\underline{H}$ product in the exit channel of MAR processes, and this part is removed from the operator $\mathcal{K}^i$ to ensure that the spectral radius $\mathrm{r}(\tilde{\mathcal{K}}^i) = \mathrm{r}(\mathcal{K}^i - \mathcal{K}^i_{\mathrm{MAR}_{\underline{\mathrm{H}}}})$ stays below one. The linear operator $\mathcal{K}^i_{\mathrm{MAR}_{\underline{\mathrm{H}}}}$ is explicitly given by the plasma state $\mathbf{P}^i$, whereas $\Gamma^{i-1}_{\mathrm{MAR}_{\mathrm{H}}}$ is calculated based on the current plasma state $\mathbf{P}^i$ and the previous neutral particle state $\mathbf{N}^{i-1}$, i.e. $\Gamma^{i-1}_{\mathrm{MAR}_{\mathrm{H}}} = \Gamma^{i-1}_{\mathrm{MAR}_{\mathrm{H}}}(\mathbf{P}^i, \mathbf{N}^{i-1})$. After splitting the transport operator, equation (3) becomes

$$\mathbf{N}^i = \left\{\Gamma\left(\mathbf{P}^i\right) + \Gamma^{i-1}_{\mathrm{MAR}_{\mathrm{H}}}\right\}\left(\mathbb{1} - \tilde{\mathcal{K}}^i\right)^{-1} \tag{5}$$

in which the above-mentioned problem of criticality has been eliminated, which is guaranteed by removing more atoms than are actually produced in the MAR processes (see below).

Our 'prediction-correction' method proposed in the present paper then consists of processing the $\underline{\mathrm{H}}$-removing operator $\mathcal{K}^i_{\mathrm{MAR}_{\underline{\mathrm{H}}}}$ and preparing the external particle source term $\Gamma^i_{\mathrm{MAR}_{\mathrm{H}}}$ for calculating $\mathbf{N}^{i+1}$ in the subsequent iteration step. Since only two iteration steps are involved, we omit the index for the former iteration step and only use the index '1' to mark the latter iteration step. We start with $\mathcal{K}_{\mathrm{MAR}_{\underline{\mathrm{H}}}}$ and continue with our strategy of symbolic formulation by letting $\mathcal{K}_{\mathrm{MAR}_{\underline{\mathrm{H}}}}\mathbf{N} = nR_{\mathrm{mar}}(\boldsymbol{x}) \cdot f_{\underline{\mathrm{H}}}(\boldsymbol{v})$ with $R_{\mathrm{mar}} = n_{\mathrm{H}_2}(\langle\sigma v\rangle_{cx} + \langle\sigma v\rangle^{\mathrm{da}}_{\mathrm{mar}})$, where n and n_{H_2} are the plasma and molecule density, and $\langle\sigma v\rangle_{cx}$ and $\langle\sigma v\rangle^{\mathrm{da}}_{\mathrm{mar}}$ are the rate coefficients of the CX-reaction in the CX-MAR chain and the DA-MAR cascade (DA followed by MN), respectively. $f_{\underline{\mathrm{H}}}(\boldsymbol{v})$ is the normalized velocity space distribution function of the resulting $\underline{\mathrm{H}}$-atoms. As already mentioned in the preceding section, it is assumed here for simplicity (and is physically rather well justified at least for the H_2^+ MAR part) that the $\underline{\mathrm{H}}$-atom carries the momentum and energy of the former proton, which means that $f_{\underline{\mathrm{H}}}(\boldsymbol{v}) = f_{\mathrm{H}^+}(\boldsymbol{v})$, where $f_{\mathrm{H}^+}(\boldsymbol{v})$ is a shifted Maxwellian of the former protons. The $\underline{\mathrm{H}}$ atoms resulting from the CX reaction and the MN process are removed and the removal rate nR_{mar} is recorded as a prediction, which is then re-scaled in EMC3 in the next EMC3-Eirene iteration loop. There EMC3 implicitly re-calculates the removal rate based on R_{mar} only, rather than using the Eirene prediction of nR_{mar} as an explicit sink term in the ion continuity equation. This correction procedure will be described in more detail in section 3.2. The corrected result is n^1R_{mar}, which is then defined as an 'external' atom source in Eirene—$\Gamma_{\mathrm{MAR}_{\mathrm{H}}} = n^1R_{\mathrm{mar}}(\boldsymbol{x}) \cdot f^1_{\mathrm{H}}(\boldsymbol{v})$ (in accordance with the symbolic formulation of $\mathcal{K}_{\mathrm{MAR}_{\underline{\mathrm{H}}}}\mathbf{N}$), where $f^1_{\mathrm{H}}(\boldsymbol{v})$ is the distribution of the emitted atoms in velocity space. It is assumed that $f^1_{\mathrm{H}}(\boldsymbol{v}) = f^1_{\mathrm{H}^+}(\boldsymbol{v})$, with the latter being the distribution of the background ions in velocity space (displaced Maxwellian) updated by EMC3.

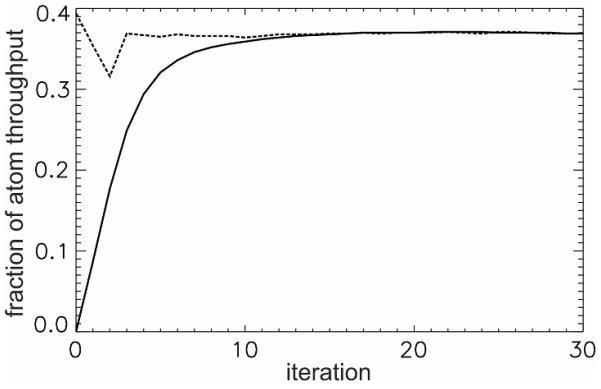

Figure 2. Atom source $\iint \Gamma_{\mathrm{MAR_H}} \mathrm{d}\boldsymbol{x}\mathrm{d}\boldsymbol{v}$ calculated in EMC3 (solid curve) iteratively approaches and finally reaches the removal rate $\iint \mathcal{K}_{\mathrm{MAR_H}} \mathbf{N} \mathrm{d}\boldsymbol{x}\mathrm{d}\boldsymbol{v}$ from Eirene (dashed).

Obviously, as $n^1 f^1_{\mathrm{H}^+}$ gets closer and closer to $n f_{\mathrm{H}^+}$ during the iteration, the added external atom source $\Gamma_{\mathrm{MAR_H}}$ will gradually equalize the removal rate $\mathcal{K}_{\mathrm{MAR_H}}\mathbf{N}$. Thus, the prediction-correction method does not alter the Eirene results beyond the range of statistical error and convergence quality, but improves the iteration stability by eliminating the possibility of runaway particle tracking. For illustrative purposes, figure 2 demonstrates the progressive convergence of the total atom source calculated by EMC3, $\iint \Gamma_{\mathrm{MAR_H}} \mathrm{d}\boldsymbol{x}\mathrm{d}\boldsymbol{v}$, and the total removal rate from Eirene, $\iint \mathcal{K}_{\mathrm{MAR_H}} \mathbf{N} \mathrm{d}\boldsymbol{x}\mathrm{d}\boldsymbol{v}$.

The atoms emerging from the ordinary EIR processes also follow the velocity space distribution of the background ions, as do the MAR atoms re-introduced into Eirene. These atoms are therefore merged into a single atom source, and subsequently launched in Eirene via the numerical tool developed for EIR [3]. They are sampled uniformly from each cell or the cell section facing the plasma when it is cut by a PFC. It is worth noting that the implementation of the prediction-correction method does not involve any modification of the Eirene source, but only minor changes to the Eirene input file.

Note that R_{mar} includes only the charge-exchange process of the CX-MAR chain, and therefore R_{mar} is not the actual total MAR rate but the rate coefficient of conversion of protons to hydrogen atoms during the CX and MN reactions. Consequently, more atoms are removed than the actual number of CX-MAR products due to the multiple competing H_2^+-elimination processes (section 2). The reason for breaking down the CX-MAR chain already at the CX-process is as follows. Unlike the DA-MAR chain, where the conversion of ion to atom occurs in the second step and the resulting atom can be removed as desired, the ion-atom conversion takes place in the first step of the CX-MAR chain. At this stage in the particle tracing procedure, the probability of the resulting H_2^+ ion undergoing the subsequent dissociative recombination remains undetermined. An analogous strategy to that used for the DA-MAR could also be developed for application to the CX-MAR; however, this would require modifications of the original source code of Eirene, which are avoided in this work. While not a prerequisite, this development would undoubtedly facilitate a more transparent decomposition of the various atomic processes.

3.2. The extended EMC3-Eirene model

While the Eirene code itself remains the same and is operated with only slightly modified input options, the activation of the MAR processes in Eirene necessitates a corresponding update of EMC3, primarily involving the incorporation of the MAR-related particle, energy, and momentum sources within the fluid model. The new version of the EMC3 code addresses the extended fluid equations as follows:

$$\nabla \cdot \left(n u_\parallel \boldsymbol{b} - D \boldsymbol{b}_\perp \boldsymbol{b}_\perp \cdot \nabla n \right) = S_{\mathrm{ion}} + n^0 R_{\mathrm{mar}} - n \left(R_{\mathrm{mar}} + R_{\mathrm{eir}} \right) \tag{6}$$

$$\nabla \cdot \left(m_{\mathrm{i}} n u_\parallel^2 \boldsymbol{b} - \eta_\parallel \boldsymbol{b}\boldsymbol{b} \cdot \nabla u_\parallel - m_{\mathrm{i}} D \boldsymbol{b}_\perp \boldsymbol{b}_\perp \cdot \nabla n u_\parallel \right) = -\boldsymbol{b} \cdot \nabla p + S_m + m_{\mathrm{i}} n^0 u_\parallel^0 R_{\mathrm{mar}} - m_{\mathrm{i}} n u_\parallel \left(R_{\mathrm{mar}} + R_{\mathrm{eir}} \right) \tag{7}$$

$$\nabla \cdot \left(\frac{5}{2} n T_{\mathrm{e}} u_\parallel \boldsymbol{b} - \kappa_{\mathrm{e}} \boldsymbol{b}\boldsymbol{b} \cdot \nabla T_{\mathrm{e}} - \frac{5}{2} T_{\mathrm{e}} D \boldsymbol{b}_\perp \boldsymbol{b}_\perp \cdot \nabla n - n \chi_{\mathrm{e}} \boldsymbol{b}_\perp \boldsymbol{b}_\perp \cdot \nabla T_{\mathrm{e}} \right) = -\kappa \left(T_{\mathrm{e}} - T_{\mathrm{i}} \right) + S_{\mathrm{ee}} + S_{\mathrm{imp}} + S_{\mathrm{eir}} \tag{8}$$

$$\nabla \cdot \left(\frac{5}{2} n T_{\mathrm{i}} u_\parallel \boldsymbol{b} - \kappa_{\mathrm{i}} \boldsymbol{b}\boldsymbol{b} \cdot \nabla T_{\mathrm{i}} - \frac{5}{2} T_{\mathrm{i}} D \boldsymbol{b}_\perp \boldsymbol{b}_\perp \cdot \nabla n - n \chi_{\mathrm{i}} \boldsymbol{b}_\perp \boldsymbol{b}_\perp \cdot \nabla T_{\mathrm{i}} \right) = +\kappa \left(T_{\mathrm{e}} - T_{\mathrm{i}} \right) + S_{\mathrm{ei}} - E_{\mathrm{i}} n R_{\mathrm{eir}}. \tag{9}$$

A detailed account of the preceding version of the EMC3 model can be found in [1]. Here, we focus only on the newly introduced terms related to volume recombination. For completeness, EIR is also included. All newly introduced terms appear on the right-hand side of the equations. Most of these terms can be identified by the subscripts 'mar' or 'eir', respectively denoting the MAR and EIR processes. The terms, S_{ion}, S_{m}, S_{ee}, and S_{ei}, represent the net results of plasma-neutral interactions for particles, momentum, and electron and ion energy. In this context, the word 'net' refers to a cumulative sum of contributions from all relevant reactions involving different particle species, as configured in the input file for running the Eirene code. To illustrate, in the presence of MAR, the particle source term S_{ion} encompasses the loss of protons. Thus, S_{ion} can have negative values in some regions and is, in fact, a sink of particles in this case. To simplify the notation, from now on we omit the index of the iteration of the current EMC3 run and use the superscript '0' to label the previous iteration. In the prediction-correction method described in the preceding section, this proton loss is $n^0 R_{\mathrm{mar}}$. The proton loss contained in S_{ion} is offset by the addition of $n^0 R_{\mathrm{mar}}$, which is subsequently treated implicitly in EMC3. This is the reason for the appearance of the term $n R_{\mathrm{mar}}$ on the right-hand side of equation (6). The sum of $S_{\mathrm{ion}} + n^0 R_{\mathrm{mar}}$ represents an absolute ion source and is everywhere positive. It should be noted that a negative absolute ion source is not yet permitted within the EMC3 code.

The associated momentum loss is treated in a manner analogous to that employed for the continuity, as seen in equation (7). There, the parallel momentum flux density $m_{\mathrm{i}} n^0 u_\parallel^0$ is taken from the previous iteration of EMC3 , while $m_{\mathrm{i}} n u_\parallel$ will be implicitly calculated in the current iteration step. In contrast, EIR is a process that involves only electrons and

ions, and thus is naturally treated implicitly in both continuity and momentum transport. More details about the EIR implementation can be found in [3].

The MAR-associated energy terms for electrons and ions are already included in S_{ee} and S_{ei}, while the EIR-related terms are calculated separately as S_{eir} and $-E_i n R_{eir}$, where E_i is the total ion energy (kinetic+thermal). The term S_{imp} represents the electron energy loss from the impurity ionization and excitation processes. Herein, they are collectively referred to as impurity radiation. Since atomic reaction coefficients in the low T_e range are very sensitive to T_e, the source terms for electron energy transport are usually linearized in T_e space and take a common form of

$$S_e = S_e^0 + \left(T_e - T_e^0\right)\frac{\partial S_e}{\partial T_e}, \tag{10}$$

where S_e stands for S_{ee}, S_{imp}, and S_{eir}. The linearization is performed only in the T_e range where $\partial S_e/\partial T_e < 0$. T_e^0 is the T_e point at which point S_e is expanded based on the previous EMC3 results. In practice, the last term in equation (10) can be weighted by any factor within the range of 0 and 1, thus allowing for an optimal efficiency for individual cases. This technical manipulation is permitted due to the fact that, as T_e converges on T_e^0, the magnitude of this term approaches zero. The necessity of energy source linearization was realized during the implementation of impurity transport and the associated radiation [13], as it was otherwise difficult to achieve convergence under high-radiation conditions. Recently, this approach has been applied to the handling of S_{ee} and S_{eir} [14], as they can be significant in tokamaks under certain conditions.

The linearization concept of a non-linear source term has two drawbacks: (1) slowdown of the convergence process and (2) introduction of additional errors. Depending on the sensitivity of S_e to T_e, the linear term can be so large that a very small change in T_e is allowed in each iteration, which may be necessary to avoid a possible runaway calculation, but could significantly slow down the iteration process. Second, equation (10) is only true if T_e converges to T_e^0. Any deviation between T_e and T_e^0 in the end can be considered as an error introduced by the linearization method, either statistically due to Monte Carlo noise or systematically due to poor convergence performance. For these reasons, it should be noted that the linearization should only be used when necessary and, if used, care should be taken to ensure that the associated errors do not affect the main results of interest.

4. Role of volume recombination in the W7-X island divertor

Until now, there has been no self-consistent numerical quantification of volume recombination in helical devices. It was previously thought that the conditions necessary for volume recombination in the island divertor were, due to the enhanced role of cross-field transport, more challenging to achieve than in tokamaks. This hypothesis was indeed supported by post-processing detachment simulation results from W7-X [12]. Nevertheless, such estimates have only been made for EIR, and never for MAR. Moreover, due to the delicate plasma state in which volume recombination is occurring, a self-consistent treatment is essential. This has now become feasible with the new code version of EMC3-Eirene.

For a first evaluation of the role of volume recombination in the island divertor, we choose here a typical detachment discharge program from W7-X - #20 180 814.25. This discharge has been well studied both experimentally and numerically [12]. It was an ECR-heated hydrogen plasma with a port power of 5.5 MW. This discharge was operated with the so-called standard divertor configuration, bounded by the iota = 5/5 island chain, which is the most-often studied magnetic configuration in terms of detachment. In the modelling, intrinsic carbon from the graphite target is assumed to be the only impurity species. Carbon atoms are sampled according to the flux deposition of the background ions on the graphite targets, accounting for chemical sputtering processes relevant for the detached plasmas of interest in this work. The total carbon yield is scaled by f_{rad}—the ratio between the volume-integrated S_{imp} in equation (8) and the total power into the computational domain, which is used as a control parameter and varied from 0.64 to 0.9. At the innermost boundary surface of the computation domain, situated approximately 8 cm inside the last closed flux surface (LCFS), the plasma density is co-varied with f_{rad} from 5 to 5.5×10^{13} cm^{-3}, in accordance with the experimental measurements. It is assumed that the anomalous diffusion coefficient, $D = 5000$ cm^2 s^{-1}, applies to both hydrogen and carbon. The cross-field heat conductivity of electrons and ions is the same, with a value of 7500 cm^2 s^{-1}. The details of the simulation setup, processes and the primary numerical results for this discharge in the absence of volume recombination can be found in [12, 15]. With the new code version, we will clarify to what extent, in which aspects and under which conditions volume recombination can alter the island-divertor plasma.

In accordance with the preceding simulations not incorporating volume recombination, the present study, which includes volume recombination, continues to assume that there are no external particle sources, no pumps, and that all PFCs, including the targets, have an ideal recycling coefficient of unity. In the presence of volume recombination, the total flux of the recycling neutrals, Γ_{recy}, can be expressed as

$$\Gamma_{recy} = \Gamma_{src} + \Gamma_{mar}^{cx} + \Gamma_{mar}^{da} + \Gamma_{eir} \tag{11}$$

where the terms on the right are, in order, the fluxes from the surface recombination on the target and the volume processes of CX-MAR, DA-MAR and EIR, respectively. It should be noted that, unlike the proton-atom conversion rate nR_{mar} discussed in the preceding section, the sum of Γ_{mar}^{cx} and Γ_{mar}^{da} in equation (11) represents the actual total atom source resulting from CX-MAR and DA-MAR, namely

$$\Gamma_{mar} = \Gamma_{mar}^{cx} + \Gamma_{mar}^{da} = \int \left(nR_{mar}^{cx} + nR_{mar}^{da}\right) \mathrm{d}\boldsymbol{x} \tag{12}$$

where $R_{mar}^{cx} = n_{H_2}\langle\sigma v\rangle_{mar}^{cx}$ and $R_{mar}^{da} = n_{H_2}\langle\sigma v\rangle_{mar}^{da}$. Accordingly, the ionization of the recycling neutrals specified in equation (11) is given by $S_{ion} + n^0(R_{mar}^{cx} + R_{mar}^{da})$, instead

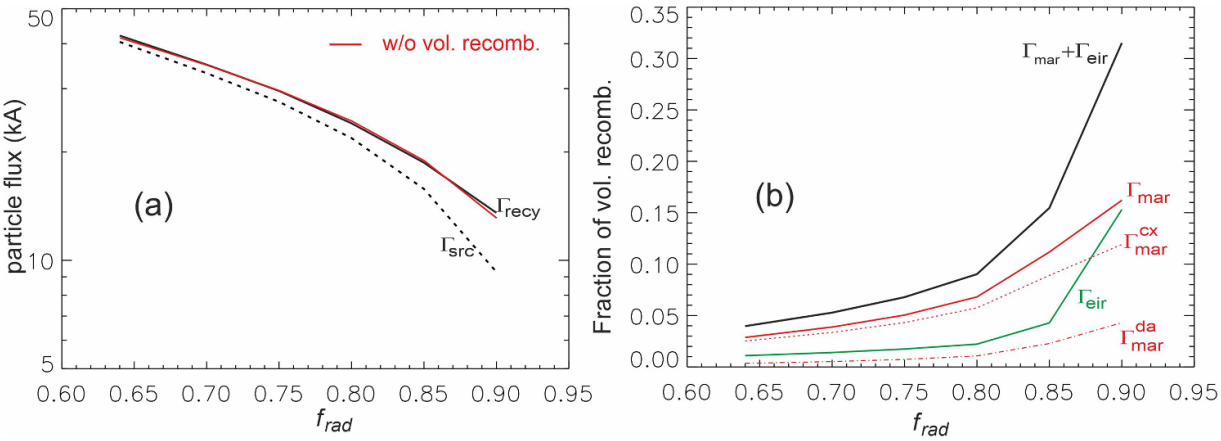

Figure 3. (*a*) The total recycling flux (black solid) and the recycling flux from the targets (black dashed) in the presence of volume recombination as a function f_{rad}. The red solid curve is the total recycling flux in the absence of volume recombination. (*b*) f_{rad}-dependence of the fractions of contribution from different reaction processes.

of $S_{ion} + n^0 R_{mar}$ in equation (6). In the following, the term $S_{ion} + n^0(R^{cx}_{mar} + R^{da}_{mar})$ is referred to as the ionization source. Its volume integration is equal to the total recycling flux, Γ_{recy}.

Figure 3 depicts the results of the simulations, using f_{rad} as an independent parameter. The red solid curve in panel (*a*) on the left represents the total recycling flux in the absence of volume recombination, serving as a reference. In this instance, $\Gamma_{recy} = \Gamma_{src}$, meaning that all neutral particles are recycled from the target. Turning on the volume recombination processes results in an overall reduction in Γ_{src}, with the effect increasing at higher f_{rad} values, while the total recycling flux Γ_{recy} remains almost unchanged. In fact, our earlier work [12] already assumed that volume recombination should not significantly change the total recycling flux. In the high radiation range, the power balance is dominated by impurity radiation and hydrogen ionization, and the electron energy cost per ionization is almost a constant. Therefore, for a given f_{rad}, the total ionization source is determined by the remaining power, regardless of where the neutral particles are recycled (from surface or volume recombination). As will be shown later, the ionization cost actually increases slightly in the presence of volume recombination, but this small effect is compensated for by the heat flux to the targets.

The deviation between the black solid and dashed curve is the contribution of volume recombination, which is resolved in panel (*b*) on the right. As already indicated in figure 3(*a*), the total contribution of volume recombination is relatively small. This is further elucidated by the black solid curve in figure 3(*b*), which represents the total contribution of volume recombination. It should be noted that all particle fluxes depicted in figure 3(*b*) are presented as a portion of the total flux Γ_{recy}. At f_{rad} below 0.8, the total contribution of volume recombination is less than 10% of Γ_{recy}. There is a rapid increase in the volume recombination contribution at $f_{rad} > 0.8$, but it remains limited to approximately 30% even at $f_{rad} = 0.9$. At this f_{rad} point, the majority of the radiation originates from closed field lines, as will be demonstrated later.

The CX-MAR process is primarily responsible for the reduction of Γ_{src}. Its contribution is approximately three times

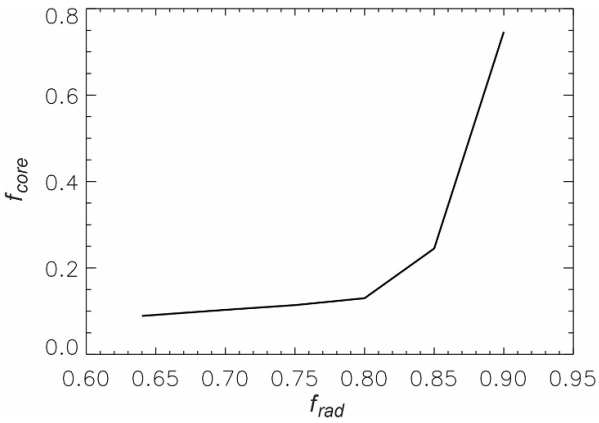

Figure 4. The radiation fraction within the LCFS increases rapidly at $f_{rad} > 0.8$ and behaves similarly to Γ_{eir} (see figure 3(*b*)).

that of EIR, except at the highest radiation point, where the latter slightly exceeds the former. In comparison, the contribution of DA-MAR can be considered minimal. In fact, its relatively diminished importance in comparison with the CX-MAR for a hydrogen plasma has been anticipated in figure 1. However, the relative significance of MAR (CX+DA) and EIR for the island divertor is not readily apparent prior to the conduction of 3D simulations.

It would be interesting to ascertain whether the rapid increase in the total volume recombination rate at f_{rad} above 0.8 is a direct consequence of the increase in f_{rad} or it is a result of the associated radiation location. In this f_{rad} range, the 3D simulations also produce a rapid growth in the portion of radiation within the confining area, as displayed in figure 4. The fraction of radiation inside the LCFS, f_{core}, increases significantly at f_{rad} values exceeding 0.8, as the radiation layer is entering the confinement region. The behaviour of f_{core} depicted in figure 4 exhibits similarities to that of the total recombination rate illustrated in figure 3(*b*), especially to that of the EIR. It appears that intense radiation on closed field lines facilitates the EIR process. One of the most plausible reasons is that radiation condensation on closed field lines favours the

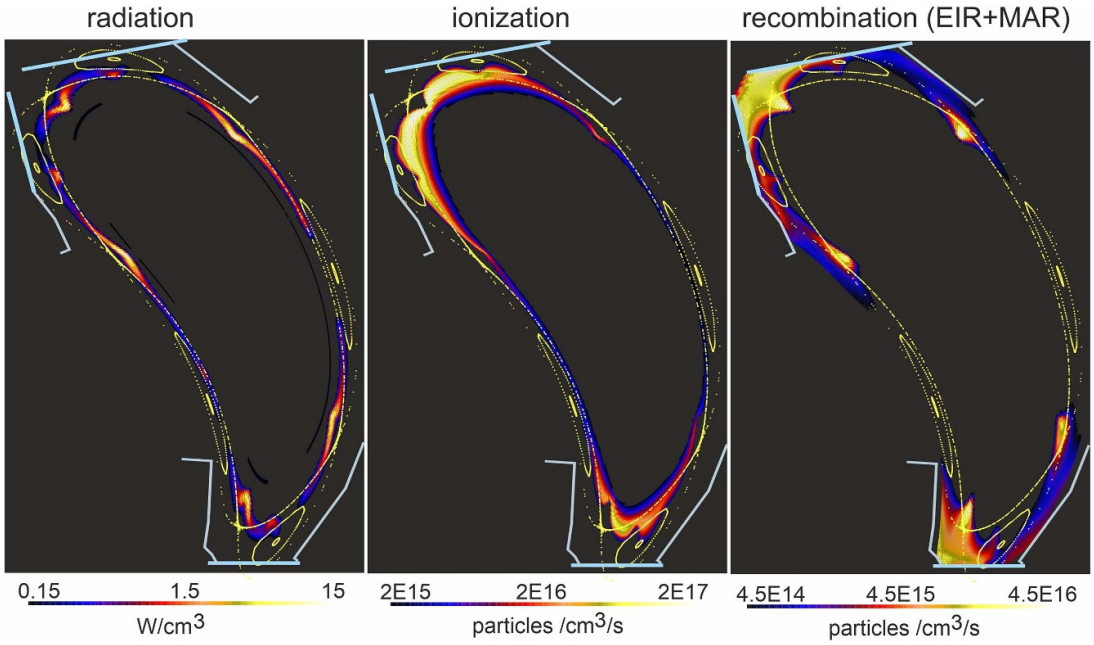

Figure 5. Distributions of (*a*) carbon radiation, (*b*) hydrogen ionization, and (*c*) volume recombination at $\phi = 12$ degrees. The three thick lines indicate three targets (two above and one below), while the thin lines indicate baffle plates. The Poincare plots illustrating the $\iota = 5/5$ island structure are generated from the vacuum field.

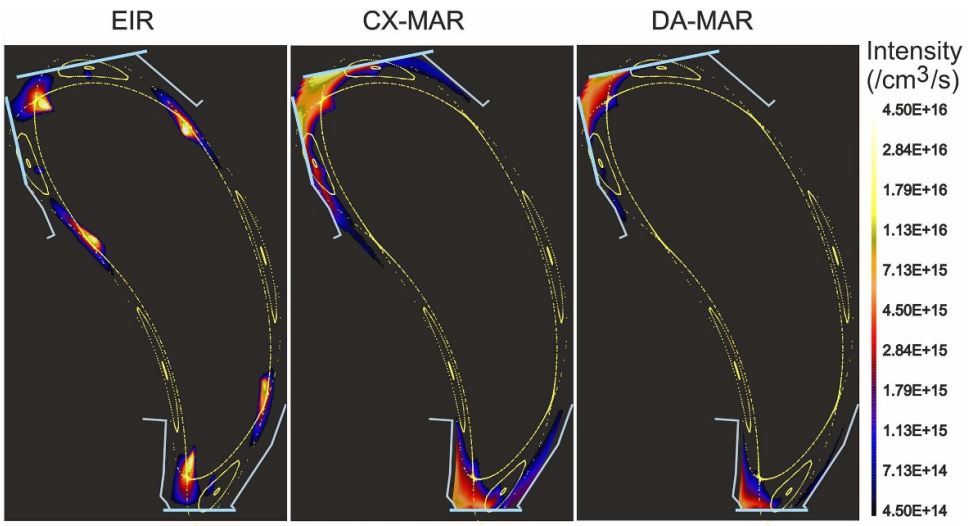

Figure 6. The location of various volume recombination processes in real space. The EIR is correlated with impurity radiation, whereas the MARs are controlled by molecule density.

build-up of plasma density due to the absence of a parallel particle transport channel. A comprehensive understanding of this point is the subject of ongoing research.

Figure 5 depicts, from left to right, the distributions of carbon radiation, the total hydrogen ionization and volume recombination for the $f_{\mathrm{rad}} = 0.9$ case. The contour plots are presented at a toroidal position situated approximately at the centre of the strike line on the upper horizontal target. In the vicinity of this ϕ-location, plasma-surface interaction occurs predominantly at the upper divertor, as evidenced by the ionization distribution in the middle panel of figure 5. Due to the high radiation level, the radiation layer penetrates into the confinement area, exhibiting a radiation pattern that is closely correlated with the X-point geometry, known as X-point radiation (XPR) [16]. The magnetic islands at the edge are too cold for ionization, so it mainly occurs around the LCFS. The recycling neutrals are confined to the region further downstream between the targets and the ionization zone as a consequence of elastic plasma-neutral collisions.

The volume recombination (CX-MAR+DA-MAR+EIR) exhibits a distribution pattern that reflects both the radiation pattern and the distribution of recycling neutrals, more precisely the molecule density. For clarity, the various recombination processes are resolved and illustrated in figure 6. The

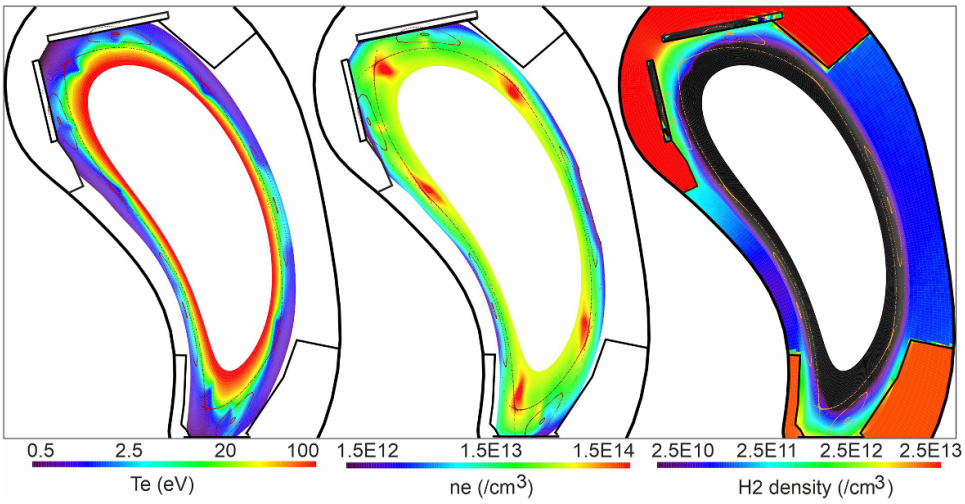

Figure 7. From left to right: the distributions of T_e, n_e and hydrogen molecule density. In contrast to figures 5 and 6, a different colour table is used here and more detailed structures of the in-vessel components are shown to highlight the molecule distribution.

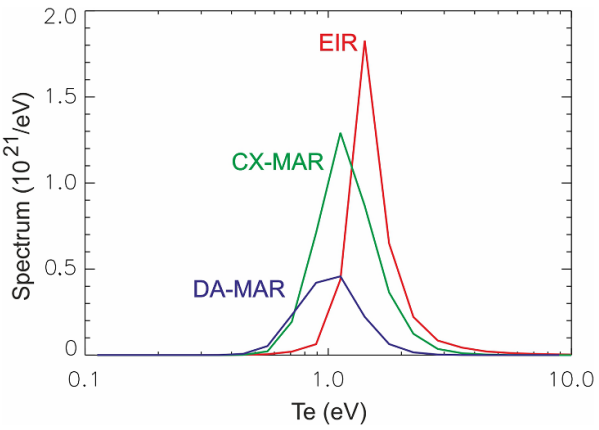

Figure 8. T_e-spectrum of the EIR, CX- and DA-MAR processes for one of the ten identical divertor modules in W7-X.

distributions of the various recombination processes can be explained with the help of figure 7. The process of EIR necessitates the presence of a dense and cold plasma that exists in the radiation zone, figure 7. This is why there is a strong correlation between EIR and carbon radiation. In contrast, the MAR processes require the participation of molecules that are located downstream in the vicinity of the target, as shown in figure 7. The DA-MAR process takes place further downstream, as it requires lower temperatures than the CX-MAR process—figure 1.

The atoms generated from the MAR processes are effectively confined by the divertor arrangement. However, due to the limited plasma coverage of the local divertor, the majority of EIR-induced atoms are born outside the area where the divertor acts. Consequently, these atoms can contribute to enhanced wall recycling in the main chamber, which, however, requires further investigation, particularly under conditions of higher heating power in the future.

The distributions of the various volume recombination processes in T_e space at $f_{rad} = 0.9$ are displayed in figure 8. The relative intensities, positions and distributions between the CX- and DA-MAR in T_e space can be easily understood from their rate coefficients in figure 1. In contrast, the behaviour of EIR is not to be expected from figure 1. It takes place in the T_e range above those of the CX- and DA-MAR processes due to density effects. The plasma density in the radiation zone is much higher than in the near target region where the molecules are located, which overcompensates for the temperature effect. As a result, the EIR process takes place mainly in the vicinity of the radiation zone—figures 5 and 6, even though the electron temperature there is higher than in the region of the MAR processes.

Figure 9 compares the downstream plasma density n_{ed} and temperature T_{ed} between the two f_{rad} scans with and without volume recombination. They represent the respective average values in the last cells before the target, weighted by the thermal pressure of the plasma. Volume recombination provides a volume sink for the charged particles on the way to the target, reducing the plasma density at the targets, as shown on the left in figure 9, especially in the high radiation range where volume recombination processes are more active. While the density effect can be explained intuitively, the reason why the volumetric particle processes lead to an overall decrease in T_{ed}, as shown on the right, is less transparent. To understand this point, we first examine the T_e spectrum of the ion source resulting from ionization and dissociation processes of the recycling neutrals. At $f_{rad} = 0.9$, the T_e spectra of the ionization source with and without volume recombination are illustrated in figure 10 on the left. In the presence of the volume recombination processes, the ionization source curve shifts to a lower T_e range. This is due to the fact that the dense and cold plasma where the volume recombination takes place has some confinement property for the resulting atoms. These atoms undergo a diffusion-like process as a result of charge-exchange with the background ions. The diffusivity of these atoms is proportional to the ratio of the ion temperature to ion density. The ionization of atoms at a lower temperature is more costly in terms of electron energy due to the increased

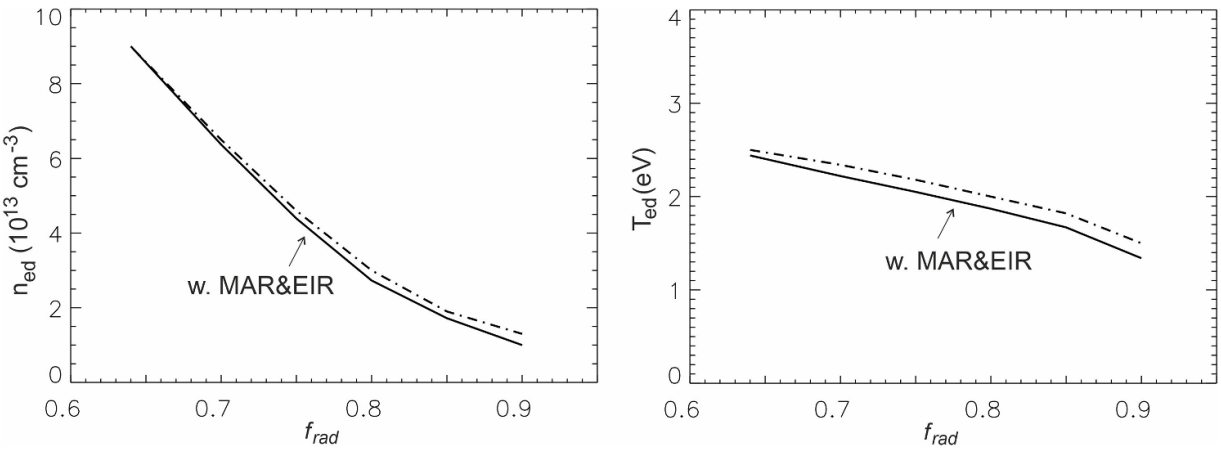

Figure 9. Comparison of $f_{\rm rad}$-dependence of $n_{\rm ed}$ (left) and $T_{\rm ed}$ (right) between the cases with (solid) and without volume recombination (dot-dashed).

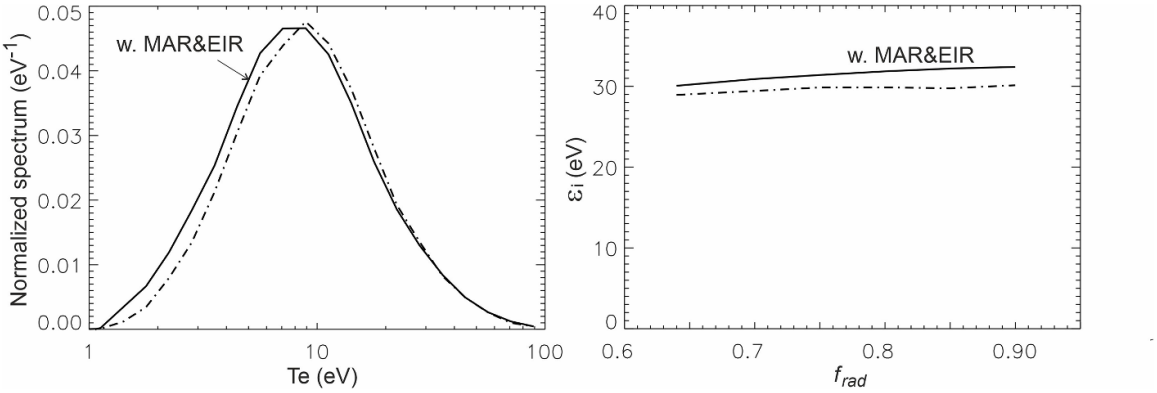

Figure 10. Left: $T_{\rm e}$ spectrum of ionization source at $f_{\rm rad} = 0.9$ with (solid) and without (dot-dashed) volume recombination. The total ionization source is normalized to unity in both cases. Right: energy costs per ionization event as a function of $f_{\rm rad}$.

probability of excitation relative to ionization. This is demonstrated in figure 10 on the right. The increased ionization cost in the presence of volume recombination is the reason for the lower $T_{\rm ed}$ values shown in figure 9.

With regard to the potential consequences of volume recombination on the performance of the island divertor, our principal concern is the peak heat load and the density of hydrogen molecules within the divertor chamber, which are depicted in figure 11. There, the peak heat load is evaluated using the Lehmer method [17] $q_{\rm peak} = \iint q^p(s){\rm d}s / \iint q^{p-1}(s){\rm d}s$ with $p = 30$, where $q(s)$ represents the heat flux density over the entire surface s of all relevant targets. The molecule density shown in figure 11 represents the mean value across the in-divertor-chamber cells. The dot-dashed lines are the results in the absence of volume recombination, which are used here as a basis for comparison.

In comparison to figure 3, which shows a clear and systematic reduction in the integrated particle flux onto the targets in the presence of volume recombination, there is no significant alteration discernible in the peak heat load or divertor molecule density in figure 11. The reasons for this are complex and require further careful analysis. In the following, we provide some intuitive explanations, while leaving a more in-depth investigation for the future.

One of the most likely explanations for the small effect on the peak heat load is that volume recombination takes place mainly in the private flux region (PFR) and around the X-points radially in front of the PFR, whereas the peak heat load occurs on the O-point side of the magnetic island, away from the PFR (see figure 25 in [12]). The XPR pattern causes the plasma to condense near the X-point, reducing the heat flux into the PFR and creating a cold, dense plasma environment that favours the volume recombination processes. In the high radiation range investigated here, the residual heat is primarily transferred radially outwards by cross-field conduction through the radiation gaps between the radiating X-points [12] and finally reaches the targets along the field lines within the magnetic islands. The cross-field conduction paths are reflected in the temperature contour plots of figure 7 by the existing 'warmer' plasma zones, which expand radially between the cold radiation zones. The topological separation between the volume recombination region and the remnant heat channel is thought to be the main cause of the weak

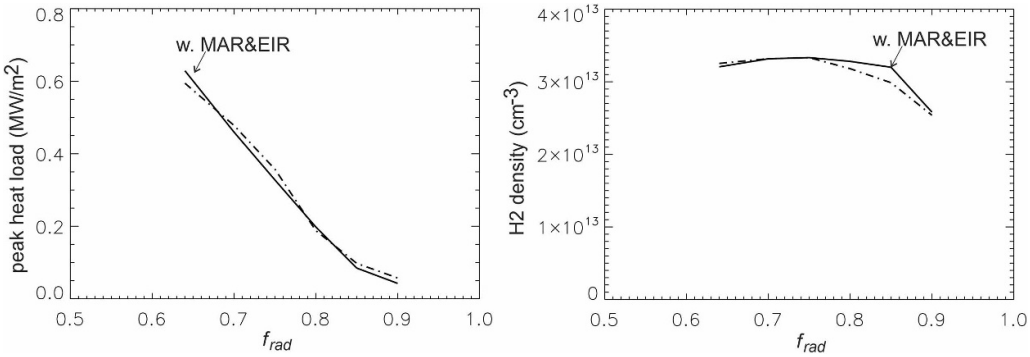

Figure 11. f_{rad}-dependence of the peak heat load (left) and the hydrogen molecule density in the divertor chamber (right) in the cases with (solid) and without volume recombination (dot-dashed).

effect of volume recombination on the peak heat load shown in figure 11.

The density of molecules in the divertor chamber is the result of a complex interplay between various factors, including the total neutral particle source, the source distribution and the transport of atoms and molecules. Under the high-radiation conditions of interest in this work, the total recycling flux is determined by the remaining power fraction available for ionizing the recycling neutrals, regardless of their origins. This explains why the total recycling flux does not change very much after the volume recombination is activated. In terms of possible source location effects, the resulting volume-neutral source in the PFR ahead of the divertor gap should favour neutral compression in the divertor chamber. Nevertheless, this advantageous effect can be diminished by the wide distribution of the volume source (in part even beyond the divertor region). In the near-target region, the transport dynamics of the neutrals are determined by charge exchange and elastic collisions, which result in a diffusion-like process. The diffusivity depends on the ratio of ion temperature and density, as well as the momentum transfer rate between ions and neutrals, in which atoms differ from molecules. In short, a comprehensive understanding of the potential consequences of volume recombination on neutral compression necessitates a decomposition of the relevant factors. However, this is challenging for the case under study, given the relatively minor role of volume recombination.

The most pronounced effects are observed in the relative population of atoms and molecules, as illustrated in figure 12 shown are the developments of the atom and molecule contents within the plasma domain (the EMC3 simulation domain) as a function of f_{rad} for the two cases with and without volume recombination. In general, the MAR processes result in a reduction in the population of molecules and an increase in the population of atoms. In comparison, the EIR process produces only a source of atoms. The less pronounced impact observed in the molecular component can be attributed to the fact that PFCs typically act as a converter of atoms to molecules, which can partially offset the loss of molecules during the MAR processes. This hypothesis is supported by the co-variation of the two red curves depicted in figure 12 for the volume recombination case. The substantial alteration in the atom population may have significant implications for relevant diagnostics.

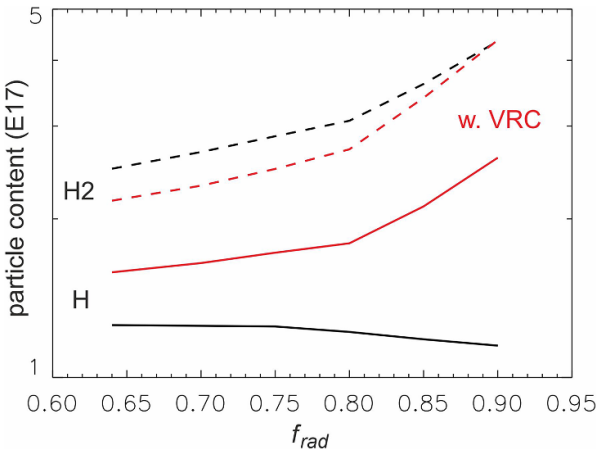

Figure 12. Changes in the atom (solid) and molecule (dashed) population within the EMC3 domain as a function of f_{rad} in the cases with (red) and without (black) volume recombination.

5. Conclusions

A new prediction-correction method has been developed to address MAR in the modelling of edge plasma transport, with the aim of avoiding potential numerical instabilities that may otherwise arise with the conventional method. This methodology has been implemented in the EMC3-Eirene code, but it can be applied to other edge transport models. The technical implementation involves the blocking of certain atomic channels in the MAR reaction chains in Eirene, a re-processing of the corresponding reaction rates in EMC3, and the re-introduction of these recalculated rates into Eirene as an external neutral particle source. Now, the EMC3-Eirene code allows for a self-consistent treatment of volume recombination, including both MAR and EIR process.

The new code version has been applied for the first time to W7-X, aiming to assess the role of volume recombination in the island divertor. A typical W7-X detachment discharge program was selected for the analysis. The simulation results

show that both EIR and MAR increase with the radiation fraction f_{rad}. Nevertheless, the total contribution remains within approximately 30% of the total recycling neutral source even at $f_{\mathrm{rad}} = 0.9$. The volume recombination does not affect the total recycling flux; rather, it reduces the particle flux on to the targets. The MAR contribution is typically around a factor of three larger than that of the EIR when the radiation is located in the edge magnetic islands outside the LCFS. However, the two contributions become comparable as the zone of intensive radiation enters the confinement region during deep detachment, which is mainly attributed to a stronger increase in the contribution of EIR. No noteworthy effects on detachment performance are observed in terms of the peak heat load on the target or the neutral pressure in the divertor chamber. Nevertheless, the volume recombination processes markedly increase the concentration of atoms in the vicinity of the targets, while slightly decreasing the population of molecules. Clarification of the implications for relevant diagnostics, as well as a more in-depth analysis of the volume recombination processes under various experimental conditions, especially for different impurity species, will be the focus of future research.

Acknowledgment

This work has been carried out within the framework of the EUROfusion Consortium, funded by the European Union via the Euratom Research and Training Programme (Grant Agreement No. 101052200 – EUROfusion). Views and opinions expressed are however those of the author(s) only and do not necessarily reflect those of the European Union or the European Commission. Neither the European Union nor the European Commission can be held responsible for them.

ORCID iDs

Y. Feng https://orcid.org/0000-0002-3846-4279
H. Frerichs https://orcid.org/0000-0002-3527-5106

References

[1] Feng Y., Sardei F., Kisslinger J., Grigull P., McCormick K. and Reiter D. 2004 *Contrib. Plasma Phys.* **44** 57–69
[2] Reiter D., Baelmans M. and Boerner P. 2005 *Fusion Sci. Technol.* **47** 172–86
[3] Frerichs H., Feng Y., Bonnin X., Pitts R., Reiter D. and Schmitz O. 2021 *Phys. Plasmas* **28** 0062248
[4] Janev R., Post D., Langer W., Evans K., Heifetz D. and Weisheit J. 1984 *J. Nucl. Mater.* **121** 10–16
[5] Lewis E. and Miller W. 1984 *Computational Methods of Neutron Transport* (Wiley)
[6] Press W.H. 1992 *The Art of Scientific Computing* (Cambridge University Press)
[7] Krasheninnikov S., Pigarov A. and Sigmar D. 1996 *Phys. Lett.* A **214** 285–91
[8] Kukushkin A., Krasheninnikov S., Pshenov A. and Reiter D. 2017 *Nucl. Mater. Energy* **12** 984–8
[9] Ohno N., Ezumi N., Takamura S., Krasheninnikov S. and Pigarov A.Y. 1998 *Phys. Rev. Lett.* **81** 818
[10] Sakamoto M. *et al* 2017 *Nucl. Mater. Energy* **12** 1004–9
[11] Reiter D. *et al* 2020 The data file AMJUEL: Additional Atomic and Molecular Data for EIRENE *Forschung. Juelich GmbH* **52425** (available at: https://eirene.de/Documentation/amjuel.pdf)
[12] Feng Y. *et al* 2021 *Nucl. Fusion* **61** 086012
[13] Feng Y., Sardei F., Grigull P., McCormick K., Kisslinger J., Reiter D. and Igitkhanov Y. 2002 *Plasma Phys. Control. Fusion* **44** 611
[14] Frerichs H., Bonnin X., Feng Y., Loarte A., Pitts R., Reiter D. and Schmitz O. 2019 *Nucl. Mater. Energy* **18** 62–66
[15] Feng Y. *et al* 2021 *Nucl. Fusion* **61** 106018
[16] Feng Y. *et al* 2024 *Nucl. Fusion* **64** 086027
[17] Lehmer D.H. 1971 *J. Math. Anal. Appl.* **36** 183–200